IJOCTA
An International Journal of
Optimization and Control:
Theories & Applications
2010

RESEARCH ARTICLE

Fractional model for blood flow under MHD influence in porous and non-porous media

Fatma Ayaz[a], Kübra Heredağ[b*]

[a] Department of Mathematics, Gazi University, Turkey
[b] Graduate School of Natural and Applied Sciences, Department of Mathematics, Gazi University, Turkey
 fayaz@gazi.edu.tr, kubra.heredag@gazi.edu.tr

ARTICLE INFO	ABSTRACT
	In this research, the Magnetohydrodynamic flow model within a porous vessel containing blood was examined. What makes this study intriguing is the inclusion of a fractional-order derivative term in the Magnetohydrodynamic flow system equations. Fractional derivatives were chosen for their ability to encompass both integer and fractional-order derivatives, leading to more realistic modeling results. The numerical solution for the partial differential equation system was obtained using the finite differences method. Solutions were derived using both central difference and backward difference approaches to enhance the reliability of the results. The Grünwald-Letnikov derivative approach was employed for the fractional derivative term, while the Crank-Nicolson method was applied for other terms. Solutions were obtained for velocity, temperature, and concentration profiles. Subsequently, a thorough analysis was conducted to investigate variations in these solutions for changing values of significant flow parameters such as Hartmann number, Grashof number, solute Grashof number, a small positive constant, radiation parameter, Prandtl number, and Schmidt number. Additionally, the study analyzed changes in the fractional derivative order. Finally, the impact of flow parameters on flow in a non-porous medium was investigated, and the results were presented graphically. The study highlighted the significant effects of various parameters on blood flow.

1. Introduction

The blood vessels should allow a sufficient amount of blood flow. However, when the vessels are not permeable enough and the blood flow rate changes, circulation disorders occur. As a result, the tissues surrounding the arteries cannot be nourished adequately, and when sufficient blood flow is not provided, organs are damaged. For these reasons, mathematical models known for blood flow are crucial for biomedical researchers, physiologists, and medical doctors [1].

When examining fluids from a fluid mechanics perspective, blood is generally defined as a non-Newtonian fluid. Studies have shown that blood flow can be described as Newtonian when blood cells are small relative to vessel diameter and the vessels are long [2]. Non-Newtonian fluids have variable viscosity. If the shear rate reaches a certain level, viscosity decreases and stabilizes, behaving like a Newtonian fluid. Newtonian fluids have a linear relationship between the applied shear stress and the resulting deformation rate (shear rate). Fluids like water, air, and oils are examples of Newtonian fluids, and their viscosity only changes with temperature [3].

Biomagnetic fluids are physiological fluids influenced by the presence of magnetic fields. The most characteristic biomagnetic fluid that can be considered a magnetic fluid is blood, as it contains hemoglobin molecules found in high concentrations, particularly in mature red blood cells,

*Corresponding Author

which are iron oxides. Nowadays, biocompatible magnetic materials are used in magnetic hyperthermia, where some very special magnetic particles are pushed into the blood. One method currently in use for treating tumors is to place a magnet near the tumor to capture magnetic particles in the tumor region. In the presence of an applied magnetic field, these particles act as heat sources. With this process, tumor treatment becomes more sensitive to radiotherapy and chemotherapy. Another application of magnets is occlusion, which prevents agents from reaching the tumor region, thus reducing blood flow [4]. This important field has attracted the interest of researchers, especially in the field of biomedical engineering and medical technology, due to its physiological applications during surgery, reducing blood flow, separating red blood cells from blood, and drug targeting.

Mathematical modeling is crucial for solving problems encountered in daily life in physics and engineering applications. Models often involve linear and nonlinear differential equations of integer order. However, in recent years, it has been suggested that these models may be insufficient to describe certain phenomena, and models involving fractional-order derivatives may be more realistic. Fractional calculus is considered effective in analyzing complex cases, including disease models, and plays a significant role in incorporating material memory effects [5]. In industry, fractional mathematics is preferred because it is more successful in modeling real systems compared to classical mathematics [6].

Fluid mechanics studies complex nonlinear systems that arise in various branches of science and often require simplification of models. On the other hand, research suggests that fractional-order models may offer more accurate representations of real-life problems compared to integer-order models [7]. Therefore, fractional differential equations have attracted the attention of many researchers in the 21st century.

The expression of fractional-order derivatives was first introduced in 1695 when L'Hôpital asked Leibniz about the meaning of D^n f for n being a fraction. Subsequently, famous mathematicians such as Euler, Laplace, Fourier, Abel, Liouville, Riemann, and Laurent were drawn to fractional calculus [8]. Euler developed the gamma function to use the factorial concept for rational numbers [9]. Thus, the gamma function became an important concept in fractional analysis. Fractional analysis has evolved to the present day. Thetheory of fractional differential equations be-comes one of the most interesting and attractivetopics and has shown an increasing development.Differential equations involving fractional orderderivatives are used to model a variety of systemshas important applied sciences and engineeringaspects [10]. Modeling utilizing fractional-order derivatives can yield more accurate results compared to integer-order derivatives. Consequently, there has been a substantial expansion in the realm of fractional research [11]. When electromagnetic fields are applied to fluid materials like blood, the flow behavior is affected. Changes in blood flow and viscosity are essential for understanding and treating certain diseases. Various studies have investigated the effects of magnetic fields on flow behavior and temperature changes. For example, J.C. Misra and his colleagues demonstrated that as the magnetic field strength increases, the fluid velocity decreases, but the temperature increases [12]. M. S. Abel and N. Mahesha showed that the combined effect of variable thermal conductivity, radiation, and uneven heat sources significantly influences the heat transfer rate at the boundary layer [13]. J.C. Misra and S.D. Adhikary found that blood viscoelasticity significantly reduces flow velocity, and wall shear stress is greatly affected by the Reynolds number [14]. V. Nagendramma and others explained various parameters related to fluid velocity, temperature, and density. They showed that as the Prandtl number increases, the temperature decreases [15]. S. Maiti and his colleagues demonstrated that fractional-degree flow models are faster than integer-order flow models, and as the Sc number increases, the density of blood decreases [16]. B. Tripathi and B. K. Sharma expressed that blood velocity is influenced by parameters, and medical doctors can take advantage of these effects in surgical procedures thanks to the magnetic field effects [17]. M. Alam and his colleagues studied heat transfer over a two-dimensional stretching plate with a viscoelastic fluid property in MHD flow [18]. A. A. Raptis examined the effects of magnetic fields on flow and the effects of porous medium permeability. It was concluded that increasing permeability increases the axial velocity [19]. S. Dinarvand and his colleagues found that as the magnetic field strength increases, blood flow velocity decreases [20]. E. Nader and his colleagues focused on blood viscosity and investigated how changes in conditions affect blood viscosity [21].

This study includes numerical solutions of the system of equations resulting from the selection of fractional-order time derivatives in an unstable

MHD blood flow model through a porous vessel. Calculations previously performed for classical derivatives (Misra et al. [22]) are obtained here with fractional-order time derivatives, and the results are compared with results containing integer-order derivatives for varying parameter values. In addition, the impact of taking the fractional time derivative in a non-porous medium on flow and how changes in the derivative order affect the flow are also explored.

2. Displayed mathematical equations

Blood flow can be considered as a flow model of fluid through a channel in fluid mechanics. Blood has a certain viscosity and is an incompressible, electrically conductive liquid. Blood flow occurs in a porous medium with time-dependent permeability, and this study examines the unstable hydromagnetic flow of a conductive fluid. Additionally, radiation is taken into account in the heat transfer within the fluid.

In the system shown in Figure 1, there is a uniform magnetic field applied in a different direction than the normal flow direction of the fluid. The magnetic Reynolds number is assumed to be very small, so the effect of the applied magnetic field can be neglected due to the induced magnetic field. The properties of the fluid are assumed to be constant except for density, which changes only with temperature. The basic flow in the system is a result of the buoyancy force due to the temperature difference between the inner medium and the wall.
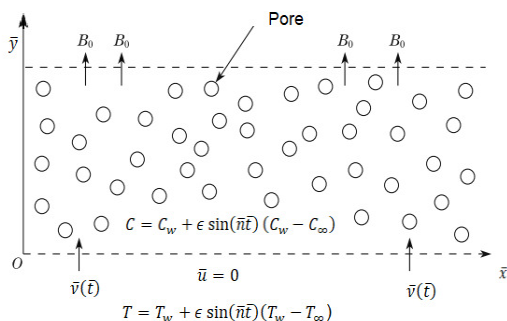

Figure 1. Physical sketch of problem

When $\bar{t} \leq 0$, it is assumed that the plate and the fluid are at the same temperature. However, when $\bar{t} > 0$, the plate's temperature is instantly raised or lowered to the surface temperature (Tw), and at the same time, the concentration of species is instantly raised or lowered to the concentration of the fluid in the plate (Cw).

$$\frac{\partial \bar{u}}{\partial \bar{x}} = 0, \qquad (1)$$

$$\frac{\partial \bar{u}}{\partial \bar{t}} + \bar{v}\frac{\partial \bar{u}}{\partial \bar{y}} = \nu\frac{\partial^2 \bar{u}}{\partial \bar{y}^2} - \frac{\nu\bar{u}}{K} + g\beta(T - T_\infty)$$
$$+ g\beta^*(C - C_\infty) - \frac{\sigma B_0^2}{\rho}\bar{u}, \qquad (2)$$

$$\frac{\partial T}{\partial \bar{t}} + \bar{v}\frac{\partial T}{\partial \bar{y}} = \frac{k_1}{\rho c_p}\frac{\partial^2 T}{\partial \bar{y}^2} - \frac{1}{\rho c_p}\frac{\partial q_r}{\partial \bar{y}}, \qquad (3)$$

$$\frac{\partial C}{\partial \bar{t}} + \bar{v}\frac{\partial C}{\partial \bar{y}} = D\frac{\partial^2 C}{\partial \bar{y}^2} \qquad (4)$$

Here, ν is the kinematic viscosity, β is the thermal expansion coefficient, β^* is the concentration-dependent thermal expansion coefficient, T is the temperature, T_∞ is the temperature of the ambient fluid, C is the concentration, C_∞ is the concentration of the ambient fluid, B_0 is the strength of the applied magnetic field, c_p is the specific heat at constant pressure, q_r is the radiative heat flux, D is the thermal molecular diffusion, and k_1 is the thermal conductivity. The term $\frac{\nu\bar{u}}{K}$' in (2) is related to the permeability of the wall. The boundary conditions are as follows:

$$\bar{u} = 0, T = T_w + \epsilon\sin(\bar{n}\bar{t})(T_w - T_\infty), \qquad (5)$$

$$C = C_w + \epsilon\sin(\bar{n}\bar{t})(C_w - C_\infty); y = 0 \qquad (6)$$

and

$$\bar{u} \to 0, T \to T_\infty, C \to C_\infty, \bar{y} \to \infty \qquad (7)$$

The relative heat flux, using the Rosseland approximation [23], is obtained as follows:

$$q_r = -\frac{4\sigma^*}{3k^*}\frac{\partial T^4}{\partial \bar{y}} \qquad (8)$$

It is assumed that the temperature difference within the flow is quite small. Therefore, T^4 can be approximated as a linear function using a Taylor series around the temperature T_∞. In this approximation, higher-order terms are neglected.

$$T^4 = 4T_\infty^3 T - 3T_\infty^4 \qquad (9)$$

With equations (8) and (9), the following equality is obtained:

$$\frac{\partial q_r}{\partial \bar{y}} = -\frac{16\sigma^* T_\infty^3}{3k^*}\frac{\partial^2 T^2}{\partial \bar{y}^2} \qquad (10)$$

Now, let's discuss dimensionless equations.

$$u = \frac{\bar{u}}{v_0}, \qquad (11)$$

$$\theta = \frac{T - T_\infty}{T_w - T_\infty}, \qquad (12)$$

$$\phi = \frac{C - C_\infty}{C_w - C_\infty}, \qquad (13)$$

The dimensionless coordinates are as follows:

$$y = \frac{\overline{y}\upsilon_0}{\nu}, \qquad (14)$$

$$t = \frac{\overline{t}\upsilon_0^2}{4\nu}, \qquad (15)$$

The dimensionless parameters are as follows:

$$K = \frac{K_0\upsilon_0^2}{\upsilon^2}, \qquad (16)$$

$$n = \frac{4\overline{n}\nu}{\upsilon_0^2} \qquad (17)$$

If we substitute equations (11) - (17) into equations (2) - (4), we obtain the following system of equations. When K is taken as the permeability of the porous medium, the equations governing the fluid motion are as follows:

$$\frac{1}{4}\frac{\partial^\alpha u}{\partial t^\alpha} + (1 + \epsilon\sin(nt))\frac{\partial u}{\partial y} = \frac{\partial^2 u}{\partial y^2} \qquad (18)$$

$$- \frac{u}{K(1 + \epsilon\sin(nt))} + Gr\theta + Gm\phi - M^2 u,$$

$$\frac{1}{4}\frac{\partial^\alpha\theta}{\partial t^\alpha} + (1 + \epsilon\sin(nt))\frac{\partial\theta}{\partial y} = \frac{(1 + Nr)}{\text{Pr}}\frac{\partial^2\theta}{\partial y^2}, \qquad (19)$$

$$\frac{1}{4}\frac{\partial^\alpha\phi}{\partial t^\alpha} + (1 + \epsilon\sin(nt))\frac{\partial\phi}{\partial y} = \frac{1}{Sc}\frac{\partial^2\phi}{\partial y^2} \qquad (20)$$

The boundary conditions are defined as follows

$$u = 0, \theta = 1 + \epsilon\sin(nt), \quad \phi = 1 + \epsilon\sin(nt),$$

$$nt = \frac{\pi}{2}, \quad y = 0, \qquad (21)$$

$$u \to 0, \quad \theta \to 0, \quad \phi \to 0, \quad y \to \infty, \qquad (22)$$

$$u_i^0 = 0.012ih(5 - ih)^4, \quad \theta_i^0 = 0.02, \quad \phi_i^0 = 0.02 \qquad (23)$$

Here, u represents the velocity of the fluid, θ denotes temperature, and ϕ represents concentration. In general, simple blood flow models consider steady flow. However, in reality, the periodic nature of the cardiac cycle leads to non-continuous pulsatile flow, and pulsatile flow has significant effects on flow velocities and stress distributions. A time step of $h = 0.025$ seconds is set, and the highest velocity for pulsatile flow is 3.072 m/s, while the lowest velocity is 0 m/s [1].

3. Numerical calculations

The finite difference approximations for the derivative terms taken with respect to y in equations, (18) - (20) given above are as follows.

$$\frac{\partial F}{\partial y} = \frac{F_{i+1}^j - F_{i-1}^j}{2h}, \qquad (24)$$

$$\frac{\partial^2 F}{\partial y^2} = \frac{F_{i+1}^{j+1} - 2F_i^{j+1} + F_{i-1}^{j+1} + F_{i+1}^j - 2F_i^j + F_{i-1}^j}{h^2}, \qquad (25)$$

In which F stands for u, θ, ϕ.

When dealing with fractional derivative terms with respect to time, the Grünwald-Letnikov [24], [25] approach is employed, while for second-order derivative terms, the Crank-Nicolson method is used. Additionally, both central differencing and backward differencing methods are utilized for first-order derivative terms. A comparison between these two methods has been conducted, with separate graphs plotted for each method.

$$\frac{\partial^\alpha F}{\partial t^\alpha} = \frac{1}{h^\alpha}\sum_{r=0}^{m+1}\omega_r^\alpha F_i^{(j-r+1)}, 0 < \alpha < 1, \qquad (26)$$

$$\omega_i^\alpha = \sum_{i=0}^{m+1}\left(1 - \left(\frac{\alpha+1}{i}\right)\right)\omega_{(i-1)}^\alpha(i-1),$$

$$\omega_0^\alpha = 1 \qquad (27)$$

After the adjustments were made, the finite difference scheme obtained is given below.

$$A_1 u_{i-1}^{j+1} + B_1 u_i^{j+1} + C_1 u_{i+1}^{j+1}$$

$$+ \frac{1}{2h^{\alpha-2}}\left(\sum_{r=2}^m u_i^{(j-r+1)}\omega_r^\alpha\right) = D1_i^j, \qquad (28)$$

$$A_2\theta_{i-1}^{j+1} + B_2\theta_i^{j+1} + C_2\theta_{i+1}^{j+1}$$

$$+ \frac{1}{2h^{\alpha-2}}\left(\sum_{r=2}^m \theta_i^{(j-r+1)}\omega_r^\alpha\right) = D2_i^j, \qquad (29)$$

$$A_3\phi_{i-1}^{j+1} + B_3\phi_i^{j+1} + C_3\phi_{i+1}^{j+1}$$

$$+ \frac{1}{2h^{\alpha-2}}\left(\sum_{r=2}^m \phi_i^{(j-r+1)}\omega_r^\alpha\right) = D3_i^j \qquad (30)$$

Here, with $f = 1 + \epsilon\sin(nt)$ and h as the time step distance, it is expressed as

$$A1 = -fh - 2, \quad B1 = 4 + \frac{1}{2h^{(\alpha-2)}}\omega_0^\alpha,$$

$$C1 = fh - 2, \qquad (31)$$

$$A2 = -2\left(\frac{1+Nr}{\text{Pr}}\right) - fh,$$

$$B2 = 4\left(\frac{1+Nr}{\text{Pr}}\right) + \frac{1}{2h^{(\alpha-2)}}\omega_0^\alpha,$$

$$C2 = -2\left(\frac{1+Nr}{\text{Pr}}\right) + fh, \qquad (32)$$

$$A3 = -\frac{2}{Sc} - fh, \quad B3 = \frac{4}{Sc} + \frac{1}{2h^{\alpha-2}}\omega_0^\alpha,$$

$$C3 = fh - \frac{2}{Sc} \qquad (33)$$

Additionally, it is expressed as

$$D1_i^j = -fh(u_{(i+1)}^j - u_{(i-1)}^j) - 4\frac{u_i^j h^2}{Kf} + 2(u_{(i+1)}^j$$
$$- 2u_i^j + u_{(i-1)}^j) + 4h^2(Gr\theta_i^j + Gm\phi_i^j - M^2 u_i^j)$$
$$- \frac{1}{2h^{(\alpha-2)}}(\omega_{(m+1)}^\alpha u_i^0 + \omega_i^\alpha u_i^j), \qquad (34)$$

$$D2_i^j = -fh(\theta_{(i+1)}^j - \theta_{(i-1)}^j) + 2(\frac{1+Nr}{Pr})(\theta_{(i+1)}^j$$
$$- 2\theta_i^j + \theta_{(i-1)}^j) - \frac{1}{2h^{(\alpha-2)}}(\omega_{(m+1)}^\alpha \theta_i^0 + \omega_i^\alpha \theta_i^j)$$
$$(35)$$

$$D3_i^j = -fh(\phi_{(i+1)}^j - \phi_{(i-1)}^j) - \frac{2}{Sc}(\phi_{(i+1)}^j - 2\phi_i^j$$
$$+ \phi_{(i-1)}^j) - \frac{1}{2h^{(\alpha-2)}}(\omega_{(m+1)}^\alpha \phi_i^0 + \omega_i^\alpha \phi_i^j)$$
$$(36)$$

(28), (30) since it is a tridiagonal linear equation system, it can be solved using the Thomas Algorithm. The matrix is a square band matrix consisting of 2500 rows and columns. Numerical solutions for a single time step were obtained using the Maple 2021 program, and changes in parameters were shown using graphs. Each of matrix calculation time about forty minutes.

4. Guidelines for tables

In this section, graphs obtained when the flow parameters in the equation system were changed are presented. The differences observed are compared.

4.1. Presentation of figures

4.1.1. Blood flow problem under the influence of MHD in porous media

Differences in the time derivative of the flow velocity, temperature, and density of blood in unstable MHD flow, which arise from taking integer derivatives of time in the previous study (see [22]) and fractional derivatives of time in this study, have been investigated. Taking α as 1 coincides with the previous study. Thus, the differences between the use of integer derivatives and fractional derivatives can be examined with the help of graphs. Furthermore, changes in the absence of porosity have been investigated. Under the given boundary conditions, $h = 0.002$, $\alpha = 0.8$, and ϵ are taken between 0.005 and 0.03, and numerical computations were performed. $j = 0$ and i are processed between 0 and 2500, and results are obtained in 2500 steps. To make the comparison more accurate, calculations were made using the parameter values specified below (see [22]).

$$M^2 = 0.5, 0.8, 1.0, 1.5, 2.0,$$
$$Gr = -20, -13.8, -10, 5, 10, 20,$$
$$Gm = 5, 10, 15, 20,$$
$$Pr = 0.025, 0.2, 0.7, 0.71, 1.5, 7.0, 10.0,$$
$$Nr = 1.0, 1.5, 2.0, 3.0, 3.5, 4.5,$$
$$Sc = 0.01, 0.05, 0.1, 0.2, 0.22, 0.5,$$
$$K = 10.0$$

In Figure 2, it is observed that as M increases, the axial velocity decreases. This is an expected result because as the M value increases, the Lorentz force increases. The Lorentz force opposes the flow.

Figure 3 is plotted using the data from the Figure 2. The only difference is that a backward difference has been used for the derivative term with respect to y. When comparing the two graphs, no significant difference is observed. This situation indicates that the obtained results are more reliable.

In Figure 4, both positive and negative values of Gr were examined. It was observed that as the Gr number decreases, meaning the amount of heat generated decreases, the velocity also decreases.

In Figure 5, when the positive values of Gm are examined, it is seen that the velocity also decreases as Gm decreases.

In Figure 6, it was observed that the velocity also decreases when the amplitude parameter ϵ decreases.

Figure 7 is plotted using the data from Figure 6. The only difference is that a backward difference has been used for the derivative term with respect to y. When comparing the two graphs, no significant difference is observed. This situation indicates that the obtained results are more reliable.

Figure 8 examines how temperature is influenced by Nr. As Nr decreases, the temperature also decreases.

Figure 9 is plotted using the data from Figure 8. The only difference is that a backward difference has been used for the derivative term with respect to y. When comparing the two graphs, no significant difference is observed. This situation indicates that the obtained results are more reliable.

In Figure 10, temperature is examined again. When Pr number increases, the temperature decreases.

In Figure 11, the change in Sc number is examined with concentration. When the channel walls

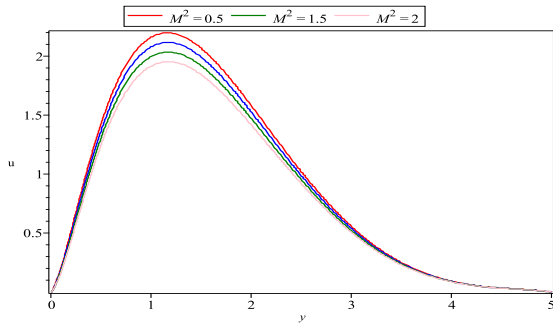cool, an increase in Sc leads to a decrease in concentration.

Figure 2. Velocity distribution for different values of M^2
(The graph plotted using central differencing method)
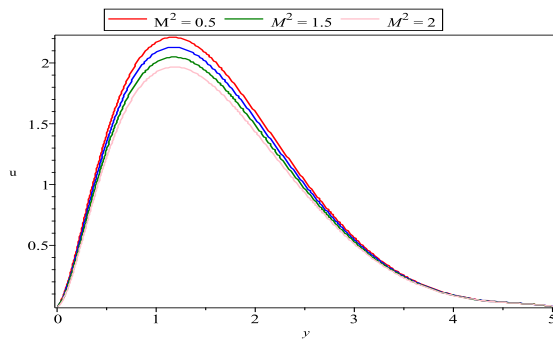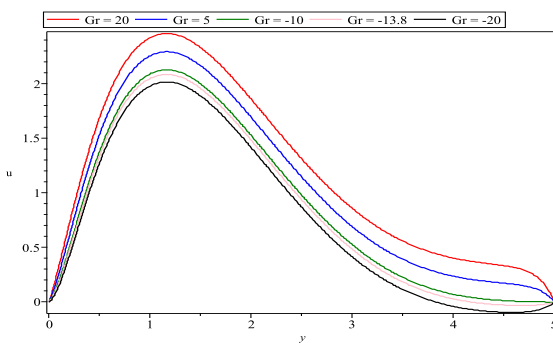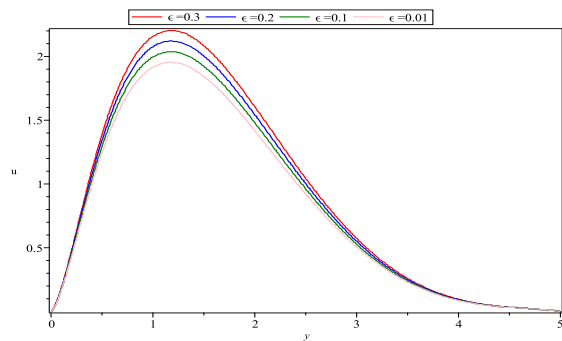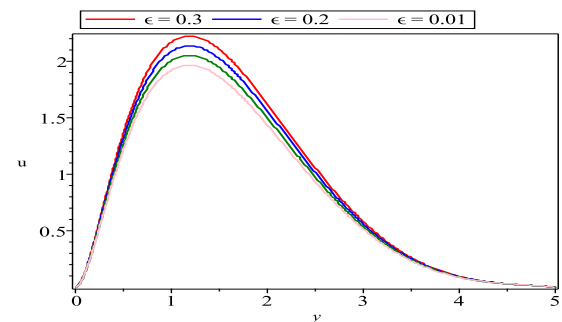$Sc = 0.22$, $Pr = 0.71$, $Nr = 1$, $Gm = 10$, $Gr = 10$, $\epsilon = 0.005$, $K = 10$, $nt = \pi/2$.

Figure 3. Velocity distribution for different values of M^2
(The graph plotted using backward differencing method)
$Sc = 0.22$, $Pr = 0.71$, $Nr = 1$, $Gm = 10$, $Gr = 10$, $\epsilon = 0.005$, $K = 10$, $nt = \pi/2$.

Figure 4. Velocity distribution for different values of Gr
$Sc = 0.22$, $Pr = 0.71$, $Nr = 1$, $Gm = 10$, $\epsilon = 0.005$, $K = 10$, $M^2 = 0.8$, $nt = \pi/2$.
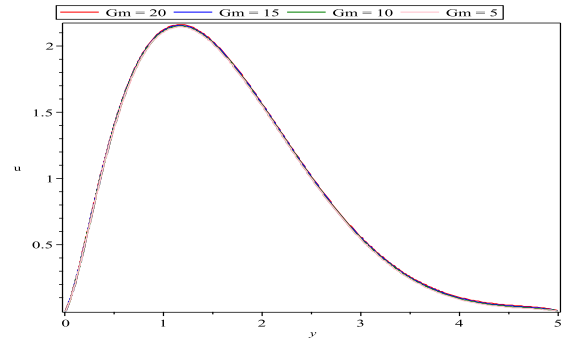
Figure 5. Velocity distribution for different values of Gm
$Sc = 0.22$, $Pr = 0.71$, $Nr = 1$, $Gm = 10$, $\epsilon = 0.005$, $K = 10$, $M^2 = 0.8$, $nt = \pi/2$.

Figure 6. Velocity distribution for different values of ϵ
(The graph plotted using central differencing method)
$Sc = 0.22$, $Pr = 0.71$, $Gr = 10$, $Gm = 10$, $Nr = 1$, $K = 10$, $M^2 = 0.8$, $nt = \pi/2$.

Figure 7. Velocity distribution for different values of ϵ
(The graph plotted using backward differencing method)
$Sc = 0.22$, $Pr = 0.71$, $Gm = 10$, $K = 10$, $Gr = 10$, $Nr = 1$, $M^2 = 0.8$, $nt = \pi/2$.
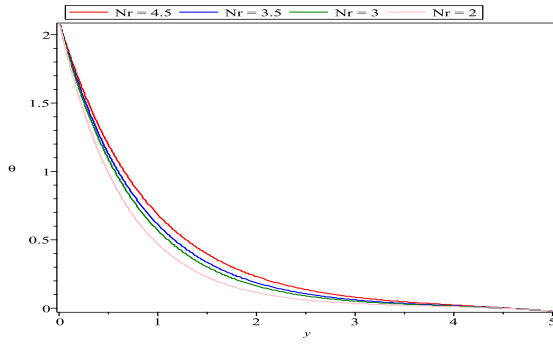
Figure 8. Temperature distribution for different values of Nr (The graph plotted using central differencing method) $Sc = 0.22$, $Pr = 0.2$, $Gm = 10$, $Gr = 10$, $\epsilon = 0.05$, $K = 10$, $M^2 = 0.8$, $nt = \pi/2$.
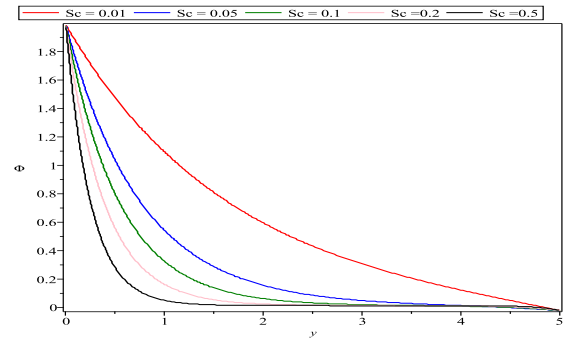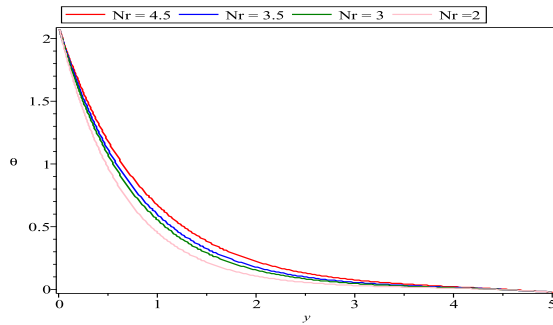

Figure 9. Temperature distribution for different values of Nr (The graph plotted using backward differencing method) $Sc = 0.22$, $Pr = 0.2$, $Gm = 10$, $Gr = 10$, $\epsilon = 0.05$, $K = 10$, $M^2 = 0.8$, $nt = \pi/2$.
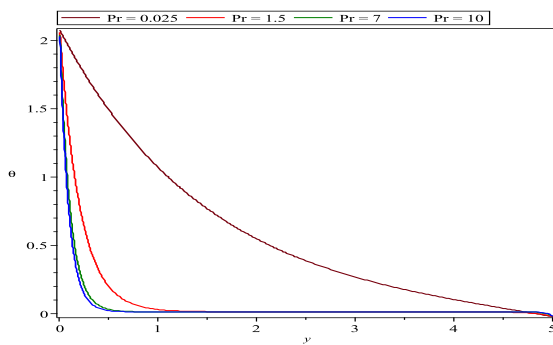

Figure 10. Temperature distribution for different values of Pr $Sc = 0.22$, $Nr = 1$, $Gm = 10$, $Gr = 10$, $\epsilon = 0.05$, $K = 10$, $M^2 = 0.8$, $nt = \pi/2$.

Figure 11. Concentration distribution for different values of Sc $Pr = 0.2$, $Nr = 1$, $Gm = 10$, $Gr = 10$, $\epsilon = 0.005$, $K = 10$, $M^2 = 0.8$, $nt = \pi/2$.

In Figures 12-19, different values of the derivative order α, with $\alpha = 1, 0.9$, and 0.8, were taken, and the changes in the results for various flow parameters were observed.

As the order of the fractional derivative approaches 1, the result obtained tends to resemble that of the classical derivative.

In Figure 12, with $Sc = 0.22$, $Pr = 0.71$, $Nr = 1$, $Gm = 10$, $Gr = 10$, $\epsilon = 0.005$, $K = 10$, $M^2 = 0.5$; and $nt = \pi/2$, the variation of the derivative order α for $\alpha = 1, 0.9$ and 0.8 was investigated. When α is taken as 0.9 and 0.8 a velocity profile similar to $\alpha = 1$ is obtained, but the flow velocity decreases.

In Figure 13, with $Sc = 0.22$, $Pr = 0.71$, $Nr = 1$, $Gr = 10$, $Gm = 20$, $\epsilon = 0.005$, $K = 10$, $M^2 = 0.8$ and $nt = \pi/2$, similar velocity profiles to those in Figure 12 were observed for varying values of the derivative order α.

Figure 14 is plotted using the data from the Figure 13. The only difference is that a backward difference has been used for the derivative term with respect to y. When comparing the two graphs, no significant difference is observed. This situation indicates that the obtained results are more reliable.

In Figure 15, with $Sc = 0.22$, $Pr = 0.71$, $Nr = 1$, $Gr = 10$, $Gm = 10$, $\epsilon = 0.3$, $K = 10$; $M^2 = 0.8$; and $nt = \pi/2$ similar velocity profiles to those in Figure 12 were observed for varying values of the derivative order α.

In Figure 16, with $Sc = 0.22$, $Pr = 0.2$, $Nr = 4.5$, $Gr = 10$, $Gm = 10$, $\epsilon = 0.05$; $K = 10$; $M^2 = 0.8$; and $nt = \pi/2$, similar velocity profiles to those in Figure 12 were observed for varying values of the derivative order α.

In Figure 17, with $Sc = 0.22$, $Pr = 0.2$, $Nr = 4.5$, $Gr = 10$, $Gm = 10$, $\epsilon = 0.05$, $K = 10$, $M^2 = 0.8$; and $nt = \pi/2$, it was observed that as α decreases, the temperature increases.

In Figure 18, with $Sc = 0.22$, $Pr = 0.025$, $Nr = 1$, $Gr = 10$,$Gm = 10$, $\epsilon = 0.05$, $K = 10$, $M^2 = 0.8$; and $nt = \pi/2$, it was observed that as α decreases, the temperature increases.

In Figure 19, with $Sc = 0.01$, $Pr = 0.2$, $Nr = 1$, $Gr = 10$, $Gm = 10$, $\epsilon = 0.05$, $K = 10$, $M^2 = 0.8$; and $nt = \pi/2$, it was observed that as α decreases, the concentration increases.

It is evident that the distributions of velocity, temperature, and concentration are significantly impacted by the fractional order parameter.
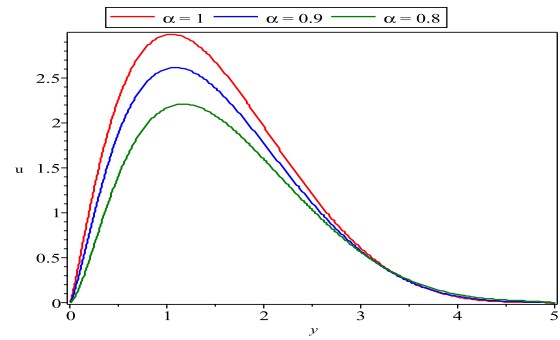
Figure 14. Velocity distribution for different values of α and $Gr=20$ (The graph plotted using backward differencing method) $Sc = 0.22$, $Pr = 0.71$, $Gm = 10$, $\epsilon = 0.005$, $Nr = 1$, $K = 10$, $M^2 = 0.8$, $nt = \pi/2$.
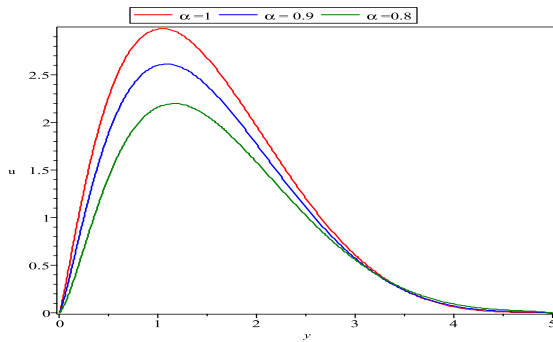
Figure 12. Velocity distribution for different values of α and $M^2=0.5$ $Sc = 0.22$, $Pr = 0.71$, $Gm = 10$, $Gr = 10$, $\epsilon = 0.05$, $Nr = 1$, $K = 10$, $nt = \pi/2$.
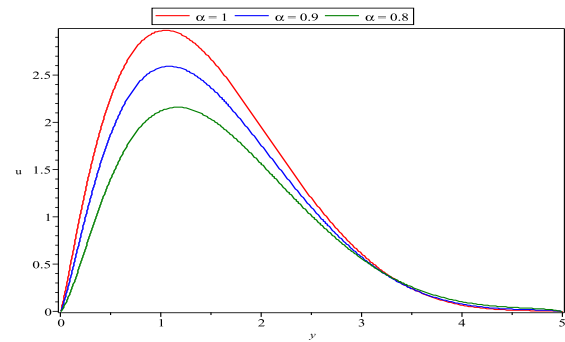

Figure 15. Velocity distribution for different values of α and $Gm=20$ $Sc = 0.22$, $Pr = 0.71$, $Gr = 10$, $\epsilon = 0.05$, $Nr = 1$, $K = 10$, $M^2 = 0.8$, $nt = \pi/2$.
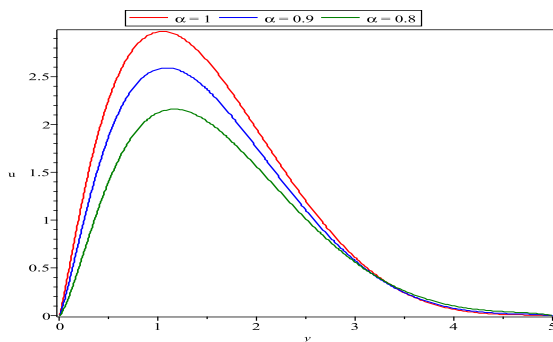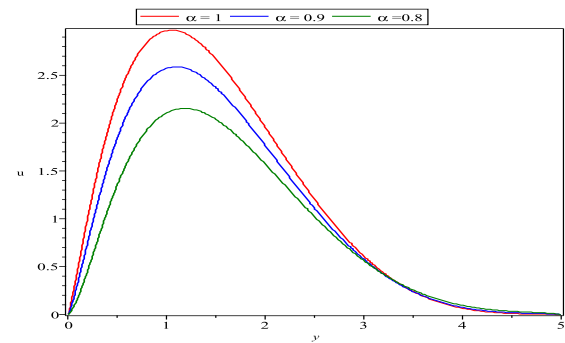

Figure 13. Velocity distribution for different values of α and $Gr=20$ (The graph plotted using central differencing method) $Sc = 0.22$, $Pr = 0.71$, $Gm = 10$, $\epsilon = 0.005$, $Nr = 1$, $K = 10$, $M^2 = 0.8$, $nt = \pi/2$.

Figure 16. Velocity distribution for different values of α and $\epsilon=0.3$. $Sc = 0.22$, $Pr = 0.71$, $Nr = 1$, $Gm = 10$, $Gr = 10$, $K = 10$, $M^2 = 0.8$, $nt = \pi/2$.
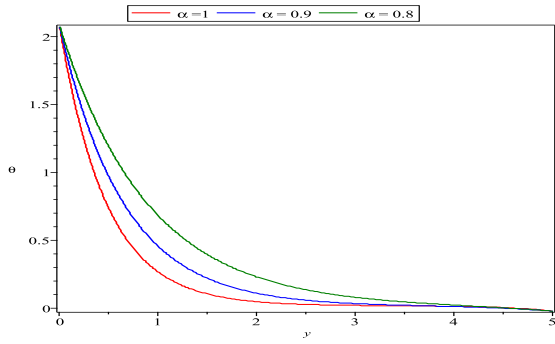
Figure 17. Temperature distribution for different values of α and Nr=4.5.
$Sc = 0.22$, $Pr = 0.2$, $Gm = 10$,
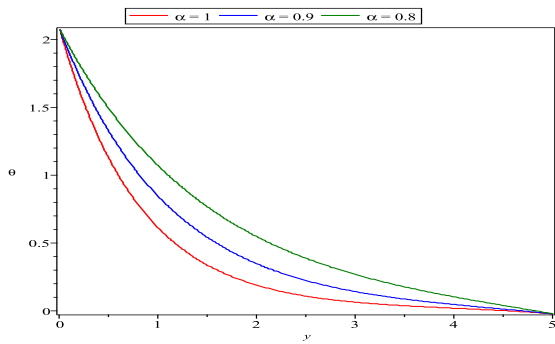$Gr = 10$, $\epsilon = 0.05$, $K = 10$,
$M^2 = 0.8$, $nt = \pi/2$.

Figure 18. Temperature distribution for different values of α and Pr=0.025.
$Sc = 0.22$, $Nr = 1$, $Gm = 10$,
$Gr = 10$, $\epsilon = 0.05$, $K = 10$,
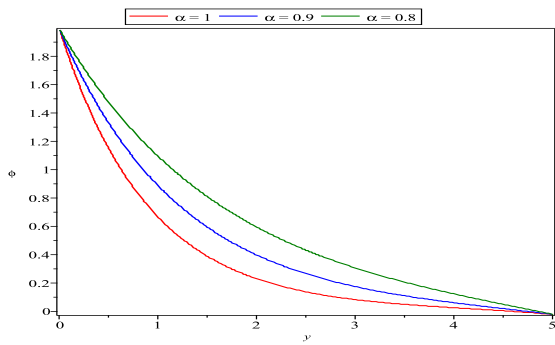$M^2 = 0.8$, $nt = \pi/2$

Figure 19. Concentration distribution for different values of α and $Sc = 0.01$,
$Pr = 0.2$, $Nr = 1$, $Gm = 10$,
$Gr = 10$, $\epsilon = 0.005$, $K = 10$,
$M^2 = 0.8$, $nt = \pi/2$

4.1.2. Blood flow problem under the influence of MHD in non-porous media

In this section, an unstable MHD blood flow problem along a non-porous vessel has been examined.

Figures 20, 21, 22, 23 and 24 show the variations in blood flow velocity. Similar to the porous medium, the velocity first increases and then decreases. The effect of parameters is very similar to that in the porous medium.

In Figure 20, it is observed that the axial velocity decreases as M^2 increases. In Figure 21, when the Gr number decreases, the velocity also decreases. Figure 22 shows that when Gm decreases, the velocity decreases similar to what is observed in Figure 21. Figure 23 is plotted using the data from the Figure 22. The only difference is that a backward difference has been used for the derivative term with respect to y When comparing the two graphs, no significant difference is observed. This situation indicates that the obtained results are more reliable. In Figure 24, it is observed that the velocity also decreases when ϵ decreases.
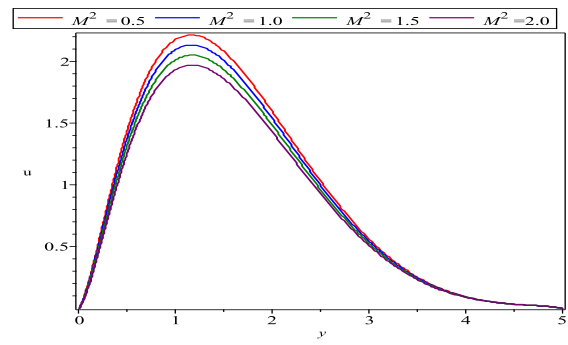

Figure 20. Velocity distribution for different values of M^2 in non-porous media
$Sc = 0.22$, $Pr = 0.71$, $Nr = 1$,
$Gm = 10$, $Gr = 10$, $\epsilon = 0.005$,
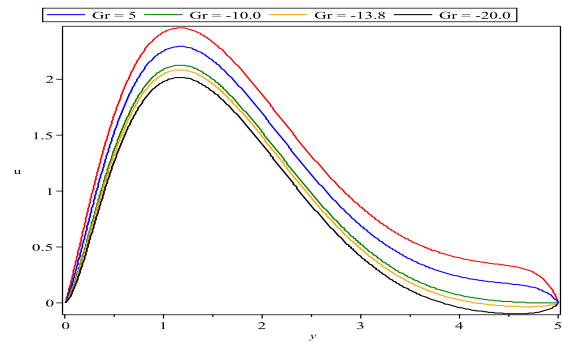$nt = \pi/2$.

Figure 21. Velocity distribution for different values of Gr in non-porous media
$Sc = 0.22$, $Pr = 0.71$, $Nr = 1$,
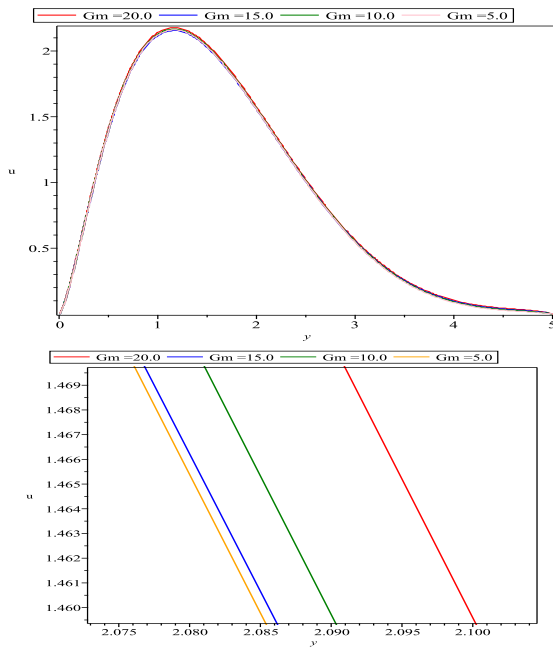$Gm = 10$, $\epsilon = 0.005$, $nt = \pi/2$.

Figure 22. Velocity distribution for different values of Gm in non-porous media
(The graph plotted using central differencing method)
$Sc = 0.22$, $Pr = 0.71$, $M^2 = 0.8$, $Gr = 10$, $\epsilon = 0.005$, $Nr = 1$, $nt = \pi/2$
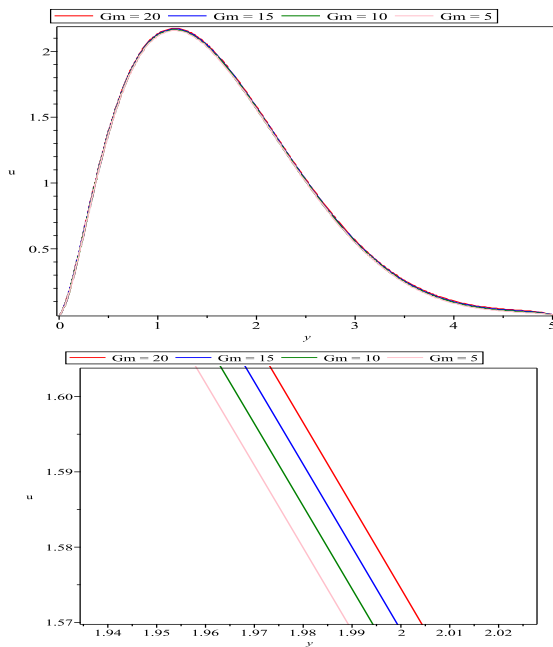
.

Figure 23. Velocity distribution for different values of Gm in non-porous media
(The graph plotted using backward differencing method)
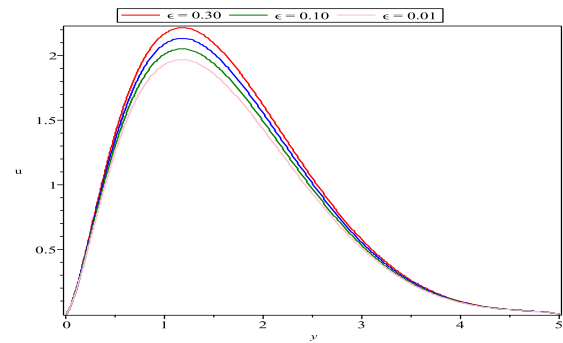$Sc = 0.22$, $Pr = 0.71$, $M^2 = 0.8$, $Gr = 10$, $\epsilon = 0.005$, $Nr = 1$, $nt = \pi/2$

.

Figure 24. Velocity distribution for different values of ϵ in non-porous media
$Sc = 0.22$, $Pr = 0.71$, $M^2 = 0.8$, $Gr = 10$, $Gm = 10$, $Nr = 1$, $nt = \pi/2$.

.

5. Conclusions

In this article, a flow model considering the MHD effect and the time-fractional derivative in a porous medium, with the fluid assumed to be blood, was initially studied. Finite differences and Grünwald-Letnikov approaches were employed in numerical computations. The research aimed to investigate whether there were differences between integer-order derivatives and fractional-order derivatives for varying parameter values. For example, the increase in the M number has led to a decrease in speed, indicating a decrease in velocity due to the effect of the magnetic field. Erdem Murat, and their colleagues have also obtained similar results. They explained this change as being caused by the retarding effect of the Lorentz force [26]. When Figure 8 is examined, it can be seen that as Nr decreases, the temperature also decreases. Similar results were obtained by C. D. K. Bansi and colleagues [27].

Also when $Sc = 0.22, Pr = 0.71, Nr = 1, Gm = 10, Gr = 10, \epsilon = 0.005, K = 10, M^2 = 0.5$ and $nt = \pi/2$, the change in the order of the derivative was examined for $\alpha = 1.0, 0.9$, and 0.8. When α decreased to 0.9, it exhibited a similar but lower velocity profile to $\alpha = 1$, and when $\alpha = 0.8$, a lower velocity profile compared to the previous case was observed. As we moved away from the integer order derivative, the flow velocity decreased.

Additionally, in this study, the non-porous medium scenario was considered and the investigation showed that there was not a significant difference in the flow model with varying parameters and fractional derivatives when the medium is non-porous.

6. Symbols

Gr,   Grashof number,

Gm,   solute Grashof number

K,   permeability parameter,

M,   Hartmann number,

Nr,   radiation parameter,

Pr,   Prandtl number,

Sc,   Schmidt number,

u,   dimensionless velocity,

ϵ,   small positive constant ($\ll 1$),

g,   acceleration due to gravity,

β,   coefficient of thermal expansion,

β^*,   coefficient of thermal expansion with concentration,

B_0,   applied magnetic field,

v_0,   scale of suction velocity (non-zero constant),

ν,   kinematic coefficient of viscosity,

σ,   electrical conductivity,

ρ,   density of fluid,

T,   temperature,

T_w,   surface temperature,

T_∞,   temperature of the ambient fluid,

C,   concentration,

C_w,   concentration of fluid at the sheet,

C_∞,   concentration of the ambient fluid,

D,   thermal molecular diffusivity,

k_1,   thermal conductivity,

K_0,   constant permeability of the medium,

n',   frequency of oscillation,

q_r,   radiative heat flux,

c_p,   specific heat at constant pressure,

σ^*,   Stefan-Boltzmann constant,

k^*,   mean absorption coefficient.

References

[1] Kucur, M. (2021). Stenoz oluşmuş y-seklinde bir damarın akışkan-katı etkileşiminin openfoam ile analizi. *Avrupa Bilim ve Teknoloji Dergisi*, (32), 872-877.

[2] Ku, D .N. (1997). Blood flow in arteries. *Annual Review of Fluid Mechanics*, 29(1), 399-434.

[3] Panton, R. L. (2024). *Incompressible Flow*, John Wiley & Sons, New York.

[4] Misra, J. C., Shit, G. C.(2019). Biomagnetic viscoelastic fluid flow over a stretching sheet. *Applied Mathematics And Computation*, 210(2), 350-361

[5] Bonyah, E., Sagoe, A. K., Kumar, D., & Deniz, S. (2021). Fractional optimal control dynamics of coronavirus model with Mittag–Leffler law. *Ecological Complexity*, 45, 100880.

[6] Yüce, A. (2022). Kesir dereceli temel transfer fonksiyon yapıları için yaklaşık analitik zaman cevabı modeli. *Adıyaman Üniversitesi Mühendislik Bilimleri Dergisi*, 9(16), 49-60.

[7] Modanlı, M., & Aksoy, A. (2022). Kesirli telegraf kısmi diferansiyel denklemin varyasyonel iterasyon metoduyla çözümü. *Balıkesir Üniversitesi Fen Bilimleri Enstitüsü Dergisi*, 24(1), 182-196.

[8] Miller K. S., & Ross B., (1993). *An Introduction To The Fractional Calculus And Fractional Differential Equations*, Wiley, New York.

[9] Çağ, C., (2010). *Gamma fonksiyonu ile ilgili bazı eşitsizlikler*, M.Sc. Thesis. Yüzüncü Yıl Üniversitesi.

[10] Modanlı, M. (2019). On the numerical solution for third order fractional partial differential equation by difference scheme method. *An International Journal of Optimization and Control: Theories & Applications (IJOCTA)*, 9(3), 1-5.

[11] Kalimuthu, K., & Muthuvel, K. (2023). A study on the approximate controllability results of fractional stochastic integro-differential inclusion systems via sectorial operators. *An International Journal of Optimization and Control: Theories & Applications (IJOCTA)*, 13(2), 193-204.

[12] Misra, J. C., Shit, G. C., & Rath, H. J. (2008). Flow and heat transfer of a MHD viscoelastic fluid in a channel with stretching walls: some applications to Haemodynamics. *Computers & Fluids*, 37(1), 1-11.

[13] Abel, M. S. & Mahesha N., (2008). Heat transfer in MHD viscoelastic fluid flow over a stretching sheet with variable thermal conductivity, non-uniform heat source and radiation. *Applied Mathematical Modelling*, 32(10), 1965-1983.

[14] Misra J. C. & Adhikary S. D. (2016). MHD oscillatory channel flow, heat and mass transfer in A physiological fluid in presence of chemical reaction. *Alexandria Engineering Journal*, 55(1), 287-297.

[15] Nagendramma V., Kumar K., Prasad D., Leelaratnam A. & Varma K. (2016). Multiple slips and thermophoresis effects of maxwell nanofluid over a permeable stretching surface in the presence of radiation and dissipation. *Journal Of Nanofluids*, 5, 1-9.

[16] Maiti, S., Shaw, S. & Shit, G. C. (2020). Caputo–Fabrizio fractional order model on MHD blood flow with heat and mass transfer through a porous vessel in the presence of thermal radiation. *Physica A: Statistical Mechanics and İts Applications*, 540, 123149.

[17] Tripathi, B. & Sharma, B. K. (2018). Effect of variable viscosity on MHD inclined arterial blood flow with chemical reaction. *International Journal of Applied Mechanics and Engineering*, 23(3), 767-785.

[18] Alam, M. J., Murtaza, M. G., Tzirtzilakis, E. E. & Ferdows, M. (2021). Effect of thermal radiation on biomagnetic fluid flow and heat transfer

over an unsteady stretching sheet. *Computer Assisted Methods in Engineering and Science*, 28(2), 81-104.

[19] Raptis, A. A. (1983). Effects of a magnetic field on the free convective flow through a porous medium bounded by an infinite vertical porous plate with constant heat flux. *Journal of the Franklin Institute*, 316(6), 445-449.

[20] Dinarvand, S., Nademi, Rostami, M., Dinarvand, R. & Pop, I. (2019). Improvement of drug delivery micro-circulatory system with a novel pattern of Cuo-Cu/blood hybrid nanofluid flow towards a porous stretching sheet. *International Journal of Numerical Methods for Heat & Fluid Flow*, 29(11), 4408-4429.

[21] Nader, E., Skinner, S., Romana, M., Fort, R., Lemonne, N., Guillot, N., Gauthier, A., Antoine-Jonville, S., Renoux, C., Hardy-Dessources, M-D., Stauffer, E., Joly, P., Bertrand, Y. & Connes, P. (2019). Blood rheology: key parameters, impact on blood flow, role in sickle cell disease and effects of exercise. *Frontiers In Physiology*, 29(11), 10, 1329.

[22] Sinha, A. & Misra, J. C. (2012). Numerical study of flow and heat transfer during oscillatory blood flow in diseased arteries in presence of magnetic fields. *Applied Mathematics And Mechanics*, 33, 649-662.

[23] Brewster, M. Q. (1992). *Thermal Radiative Transfer Properties*. John Wiley & Sons, New York.

[24] Polat, R. (2018). Finite difference solution to the space-time fractional partial differential-difference toda lattice equations. *Journal of Mathematical Sciences and Modelling*, 1(3), 202-205.

[25] Cui, M. (2009). Compact finite difference method for the fractional diffusion equation. *Journal of Computational Physics*, 228(20), 7792-7804.

[26] Erdem, M., Fırat, M., & Varol, Y. (2021). Al2O3-Su nanoakışkanının manyetik alan altında akış karakteristiklerinin sayısal analizi. *Fırat Üniversitesi Mühendislik Bilimleri Dergisi*, 33(2), 401-412.

[27] Bansi, C. D. K., Tabi, C. B., Motsumi, T. G., & Mohamadou, A. (2018). Fractional blood flow in oscillatory arteries with thermal radiation and magnetic field effects. *Journal of Magnetism and Magnetic Materials*, 456, 38-45.

Fatma Ayaz *is a professor in the Department of Mathematics at Gazi University, specializing in applied mathematics. She completed her Ph.D. at the University of Leeds (United Kingdom). Her research interests include numerical and approximate solutions of differential equations, natural sciences, engineering, and technology.*

[iD] https://orcid.org/0000-0003-4346-9821

Kübra Heredağ *is a doctoral student in the field of applied mathematics at the Mathematics Department of the Institute of Science at Gazi University. She works as a mathematics teacher at the Ministry of National Education in Ankara. She completed her undergraduate studies at Karadeniz Technical University and her graduate studies at Karabük University.*

[iD] https://orcid.org/0000-0002-1830-1093